An ab initio Study of Reduction of V_2O_5 through the Formation of Oxygen Vacancies and Li Intercalation

David O. Scanlon, Aron Walsh,† Benjamin J. Morgan, and Graeme W. Watson*

School of Chemistry, University of Dublin, Trinity College, Dublin 2, Ireland

Received: November 30, 2007; Revised Manuscript Received: April 01, 2008

Two methods of reduction of V_2O_5 have been investigated: oxygen vacancy formation and lithium intercalation. The electronic structure, geometry, and energetics of these reduced systems are examined. Oxygen vacancies in bulk α-V_2O_5 have been investigated by using gradient-corrected density functional theory (GGA) and density functional theory corrected for on-site Coulomb interactions in strongly correlated systems (GGA+U). The GGA calculation predicts a delocalized defect electronic state. This disagrees with experimental evidence, which indicates that oxygen vacancies produce a localized reduced vanadium state in the band gap. The DFT+U results for $U = 4.0$ eV are consistent with available UPS and XPS data, indicating strong localization on the vanadium atoms nearest the vacancy, and showing reduced V(IV) species. Intercalation of Li in V_2O_5, which has important potential applications in energy storage devices, is also reported at the GGA+U level, using the value of U obtained from the oxygen-deficient calculation, and localized reduction is demonstrated. These results are again in agreement with available UPS data and crystallographic data, indicating good transferability of this value of U among the systems of interest. Calculated lithium intercalation energies for both the α- and γ-V_2O_5 phases are reported, and the structure and relative stability of the deintercalated γ-V_2O_5 phase are also examined.

1. Introduction

Divanadium pentoxide (V_2O_5) is one of the most widely studied and important of the transition metal oxides. It has important applications in the selective oxidation of hydrocarbons and sulfur dioxide and the selective catalytic reduction of nitric oxide by ammonia, in addition to being an effective photocatalyst.[1,2] V_2O_5 undergoes a reversible and fast insulator−metal transition near 257 °C and thus has potential applications in write−erase media, thermally activated electrical and optical switching devices, critical temperature sensors, and light detectors [see ref 3 and references therein].

At room temperature V_2O_5 is an insulator with a band gap of ∼2.3 eV,[4] in which vanadium formally adopts its highest valence state of V(V). It crystallizes in an orthorhombic crystal structure (space group *Pmmn*), with lattice constants[5] $a = 11.512$ Å, $b = 3.564$ Å, and $c = 4.368$ Å. The primitive cell contains four V atoms and ten O atoms, corresponding to two formula units, and forms a series of layers that are perpendicular to the [001] z axis, Figure 1. Each layer consists of a periodic arrangement of edge-sharing and corner-sharing distorted VO_5 square pyramids. Pairs of pyramids point along the $-z$ direction, alternating with paired pyramids which point in the $+z$ direction. The unit cell is made up of four crystallographically inequivalent atoms: one vanadium and three oxygen atoms. These oxygen atoms are denoted in what follows as O1, O2, and O3. O1 is a terminally (vanadyl) bound oxygen, formally with a double bond to V, which is oriented almost perpendicular to the (001) plane, with a V−O interatomic distance of 1.58 Å. The bridging O2 oxygen connects two adjacent vanadium atoms with two V−O bond lengths of 1.78 Å, and O3 is a 3-fold coordinated oxygen with three V−O bond lengths of 1.88, 1.88, and 2.02 Å.[5] The distance betwen O1 and the nearest vanadium in an adjacent layer is 2.79 Å, consistent with weak noncovalent interlayer interactions which are mainly van der Waals in origin.[5]

Oxidation reactions catalyzed by transition metal oxides have long been known to be influenced by atomic scale surface structures and associated defects.[6] The generally accepted mechanism of the selective oxidation reactions that lead to functionalization of hydrocarbons is the so-called "nucleophilic" mechanism, proposed by Mars and van Krevelen, in which oxygen from the catalyst takes part in the reaction by both abstracting hydrogen atoms from the organic molecules and being incorporated into the organic species.[7,8] As a result of these steps, the transistion metal oxide is reduced through the creation of oxygen vacancies on the surface. V_2O_5 is one of the most easily reduced transition metal oxides making it a strong candidate catalyst for these reactions.[9] The identification of the oxygen that is most readily lost during reduction is a source of much debate, with O1,[10] O2,[11] and O3[12] having all been suggested as the active species. Elucidation of the active species is an important goal and thus the electronic structure and geometry of oxygen vacancies in V_2O_5 have been extensively studied experimentally.[13–17]

Vacancies generated upon reduction have been observed by various spectroscopic techniques including STM (scanning tunnelling microscopy),[14,16] ARXPS (angular resolved X-ray spectroscopy),[13] ARUPS (angular resolved ultraviolet photoemission spectroscopy),[15] TEM (transmission electron microscopy), and EELS (electron energy loss spectroscopy).[16] The general consensus is that the vanadium ions neighboring the oxygen vacancy are reduced. UPS and ARUPS data display a distinct peak +1 eV above the valence band indicating a localized reduced vanadium state.[15,17] XPS data also indicate that some surface vanadium atoms are reduced to V(IV).[17] This analysis is also consistent with previous ARXPS studies.[13]

* Corresponding aurhor. Phone: +353 1 896 1357. E-mail: watsong@tcd.ie.
† Current address: National Renewable Energy Laboratory, Golden, Colorado.

10.1021/jp711334f CCC: $40.75
Published on Web 06/07/2008

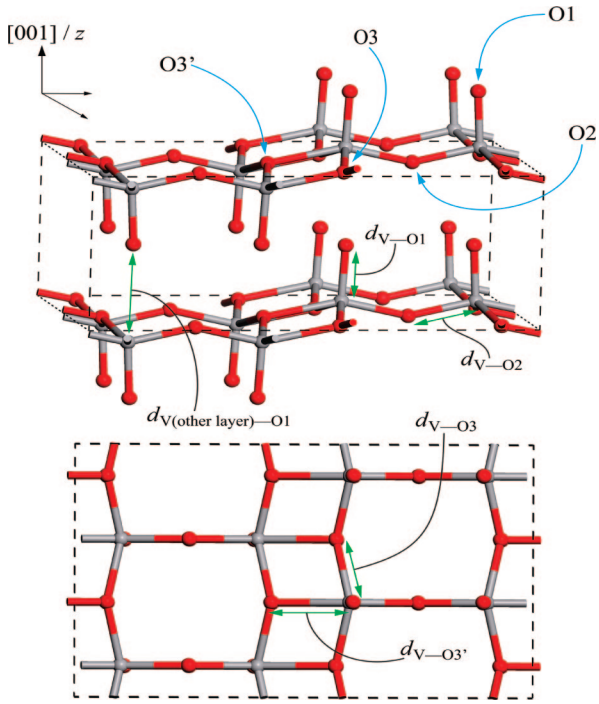

Figure 1. V_2O_5 bulk structure viewed along the [010] direction (upper panel) and the [001] direction (lower panel). V atoms are in gray and O atoms are in red. O1 is the vanadyl oxygen, O2 is a two-coordinate oxygen, and O3 is a three-coordinate oxygen. The two V−O3 distances are inequivalent and the more distant O3 is indicated here and throughout the text with a prime.

Another process resulting in the reduction of V_2O_5 reduction is Li intercalation.[18,19] This proceeds according to the electrochemical reaction

$$V_2O_5 + xLi^+ + xe^- \leftrightarrow Li_xV_2O_5$$

Photoelectron spectroscopy studies have shown that intercalation of lithium into V_2O_5 is accompanied by the appearance of a peak in the UPS spectrum at ~1.1 eV above the valence band similar to that observed for oxygen vacancy formation, and attributed to the existence of V(IV) species.[20] This behavior has potential applications in batteries and electrochromic thin film devices.[21] The system is still a source of much debate due to the existence of many complex lithiated phases, the relative stability of which depend on x and the temperature.[18] In the range $0 < x \leq 1$, the α-, β-, ϵ-, and δ-phases are all reported.[21–25] The α-$Li_xV_2O_5$ phase appears when $x < 0.1$, β-$Li_xV_2O_5$ occurs in the $0.3 \leq x \leq 0.4$ range, ϵ-$Li_xV_2O_5$ exists in the range $0.3 \leq x \leq 1.0$, and δ-$Li_xV_2O_5$ occurs in the range $0.9 \leq x < 1$. In all these cases, the phase transitions are fully reversible, and after deintercalation the thermodynamically stable α-V_2O_5 structure is recovered. When $0 < x \leq 1$, the vanadium atoms are thought to be partially reduced from V(V) to V(IV) during intercalation, based on interpretation of crystallographic data.[23,26,27] For lithium concentrations where x(Li) > 1 the δ-$Li_xV_2O_5$ phase is transformed into γ-$Li_xV_2O_5$. This is an irreversible transition[21] and upon deintercalation to $x < 1$ a metastable γ-V_2O_5 phase is recovered.[28]

The reduction of V_2O_5 has undergone extensive theoretical examination including DFT cluster models,[15,29–31] periodic DFT,[32,33] and DFT+U.[34] Hermann et al. investigated the local electronic structure of oxygen vacancies on the (001) surface using a DFT cluster model and reported that chemical reduction of neighboring vanadium atoms occurs, which was shown by the increased V 3d occupation in orbital and EDOS (electronic density of states) analysis.[29,30] However, no distinct peaks in the band gap were reported, in contrast to experimental results.[15,17]

A periodic DFT study conducted by Ganduglia-Pirovano and Sauer[32] investigated the relative stability of different reduced V_2O_5 (001) surfaces. They reported electronic structure calculations of vanadyl oxygen vacancies (O1), indicating some reduction of two neighboring vanadium atoms and further charge delocalized over the neighboring vanadium atoms. They reported a defect peak in the DOS at the bottom of the conduction band, with the conduction band crossing the Fermi level. These DOS results are again at variance with the reported spectroscopic data, which predict the defect state to be in the band gap about 1 eV above the valence band.[15,17]

Sauer and Dobler performed cluster calculations on the O1 vacancy utilizing both PBE and hybrid B3LYP functionals and found the two approaches yielded very different results.[31] Both calculations predicted that on relaxation a V−O−V bond between layers is formed, which is consistent with previous DFT calculations.[29,30,32] B3LYP showed complete localization of the excess charge on the vanadium directly neighboring the defect and the vanadium in the layer directly below,[31] while PBE showed charge delocalized over four vanadium centers. EDOS data for the PBE calculation only were reported, again describing a metallic system with the excess charge located at the bottom of the conduction band.[31] The bond formation between layers upon vanadyl vacancy formation suggests that single-layer systems are not sufficient to accurately model defects in divanadium pentoxide.[35]

Jiang et al. recently reported a DFT study of β-$Li_xV_2O_5$ (x = 0.32) and found the excess electrons gained upon intercalation of Li into the V_2O_5 system were situated at the bottom of the conduction band, which then crossed the Fermi level to give a metallic system.[36] This is again at variance with experimental data, which position the excess electrons at ~1.1 eV above the valence band[20]

It is becoming increasingly clear that standard DFT incorrectly predicts delocalized solutions in many oxides for defective states that are expected from experimental data to be localized (e.g., Li doped MgO[37,38] transition metal doped Cu_2O;[39] and oxygen vacancies in CeO_2,[40] MoO_3[41] and TiO_2[42]). The origin of this problem is the failure of the DFT exchange-correlation functional to correctly describe exchange interations. Within Hartree−Fock theory the Coulombic interaction is correctly described because the self-interaction of the electron is canceled by exact exchange. In DFT, however, the functional only contains approximate exchange, resulting in an incorrect cancellation of this self-interaction, giving rise to a so-called self-interaction error.[43–46] One approach that has been used successfully to describe such oxides is DFT+U. Within this methodology a Hubbard-like term is applied to atom-projected orbitals of interest, in this case V 3d, which introduces an energetic penalty to partial occupation. This approach is generally applicable to cases where DFT fails to give the correct localized structure, such as the present case of oxygen vacancies and Li intercalation in V_2O_5.[32,34,36]

A recent theoretical and experimental study on the electronic structure and geometry of oxygen vacancies in V_2O_5 has been undertaken by Laubach et al. [34] using DFT+U to investigate the defect site. A U value of 6.6 eV was used, which was obtained by fitting the calculated valence-band−conduction-band gap to the experimental value.[34] Analysis of the density of states shows a new feature in the energy range −6 to −5.5 eV (near

the bottom of the valence band), which was assigned to hybridization between two vanadium atoms and a terminal oxygen above the vacancy.[34] This does not agree with experimental data,[15,17] and is also at variance with resonant V 3p−V 3d photoelectron spectroscopy (ResPES) reported in the same study, which shows a peak in the density of states at ∼1 eV above the valence band.[34] We propose that an improved description of oxygen-deficient V_2O_5 can be obtained by carefully selecting a value of U such that the experimentally observed features of interest are obtained, in this case the distinct defect peak in the band gap. Furthermore, a value of U selected in this way is likely to be suitable for describing other reduced V_2O_5 systems, such as are formed upon lithium intercalation.

In the work presented here, the electronic structure, geometry, and energetics of bulk stoichiometric and oxygen-deficient V_2O_{5-x} are reported, calculated by using both gradient-corrected DFT (GGA) and DFT+U (GGA+U), using a value of U that results in an experimentally consistent description of the oxygen-reduced system. GGA+U with the same U has also been used to calculate the structure and energetics of Li intercalation of V_2O_5, in both the α-$Li_xV_2O_5$ phase ($x = 0.28$) and the γ-$Li_xV_2O_5$ phase ($x = 1$), and the transferability of a single U value is judged on the degree of agreement with experimental data.

2. Methods

For all calculations the periodic DFT code VASP[47,48] was employed, in which valence electronic states are described within a plane wave basis set. Exchange and correlation were treated by using the Perdew−Burke−Ernzerhof[49] gradient corrected functional. The projector-augmented wave (PAW) method[50] was used to describe the interaction between the core (V:[Be] and O:[He]) and valence electrons. All calculations were fully spin polarized to allow the excess electrons introduced upon reduction, either by oxygen removal or lithium intercalation, to be correctly described.

To calculate equilibrium lattice parameters for the chosen model, structural optimizations of bulk V_2O_5 were performed at a series of volumes, in each case allowing the atomic positions, lattice vectors, and cell angles to relax while holding the total volume constant. The resulting energy volume curves were fitted to the Murnaghan equation of state to obtain the equilibrium bulk cell volume.[51] This approach was taken to avoid the problems of Pulay stress and changes in basis set that accompany volume changes in plane wave calculations. The system was checked for convergence with respect to k-point sampling and plane wave energy cutoff. A cutoff of 500 eV and a k-point sampling of $2 \times 2 \times 2$ were found to be sufficient. The structural optimizations were deemed to be converged when the force on every ion was less than 0.01 eV $Å^{-1}$. The minimum energy GGA and GGA+U lattice parameters were then used for all subsequent reduced system calculations, which were performed using the same calculation parameters, and with the same convergence criterion. This approach approximates the limit of isolated defects in an infinite bulk, in contrast with modeling a periodic array of defects at a finite concentration with appropriate relaxation of the crystal lattice. Convergence with supercell size was examined by comparing O1 vacancy formation energy within GGA+U in a $1 \times 4 \times 4$ supercell and $1 \times 3 \times 3$ supercell. The vacancy formation energy is within 0.01 eV in the two systems, indicating that a $1 \times 3 \times 3$ supercell is sufficiently large for these defect calculations.

GGA calculations with equivalent convergence criteria and calculation parameters were performed on metallic lithium and molecular oxygen, so that consistent energies could be used in the calculation of defect formation energies.

TABLE 1: Comparison of Orthorhombic Lattice Constants a, b, c of Bulk V_2O_5 Obtained from Experimental Measurement versus Those from the Current GGA and GGA+U Calculations[a]

	exptl[8]	GGA	GGA+U
a	11.512	11.542 (+0.26%)	11.496 (−0.14%)
b	3.564	3.567 (+0.08%)	3.630 (+1.85%)
c	4.368	4.858 (+11.22%)	4.804 (+9.98%)

[a] The percentage values give the relative deviation from the experimental value. All values are given in Å.

TABLE 2: Calculated V−O Bond Distances for the Bulk V_2O_5 Structure[a]

	bulk (exptl[5])	bulk GGA	bulk GGA+U
d_{V-O1}	1.581	1.608 (+1.7%)	1.602 (+1.3%)
d_{V-O2}	1.780	1.792 (+0.7%)	1.805 (+1.4%)
d_{V-O3}	1.881	1.889 (+0.5%)	1.915 (+1.3%)
$d_{V-O3'}$	2.022	2.040 (+0.9%)	2.018 (−0.2%)
$d_{V(other\ layer)-O1}$	2.793	3.252 (+16.0%)	3.204 (+14.0%)

[a] All values are given in Å. The percentage values give the relative deviation from the experimental value.

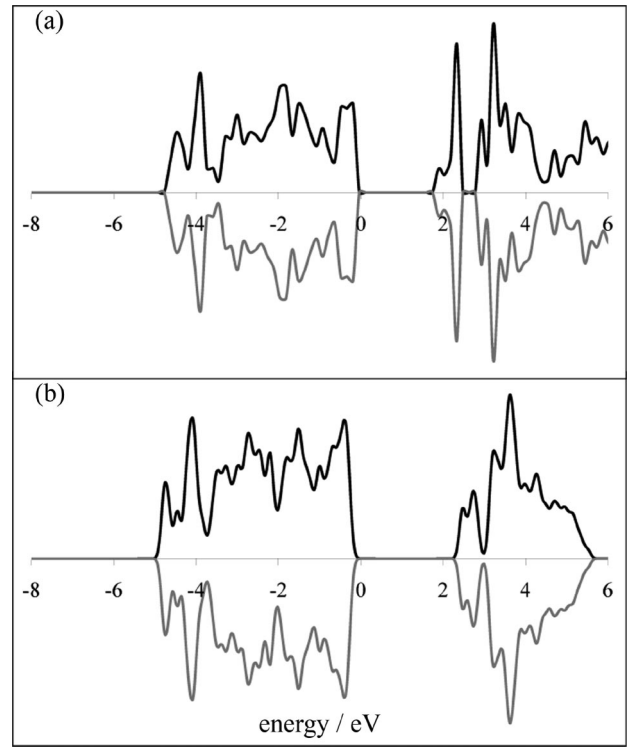

Figure 2. Calculated electronic density of states for stoichiometric V_2O_5, using (a) GGA and (b) GGA+U. In both cases the zero is aligned with the uppermost occupied state at the top of the valence band. The curves above and below the abscissa respectively show the spin-up and spin-down states (black spin-up, gray spin-down).

3. Results

3.1. Bulk V_2O_5. Table 1 shows the calculated lattice parameters for the GGA and GGA+U calculations. The value of U is 4.0 eV, with the rationale behind this choice discussed in the next section. In both cases the c vector is greatly overestimated, which is a known error of DFT.[52,53] The interaction between the ab layers is van der Waals in origin,

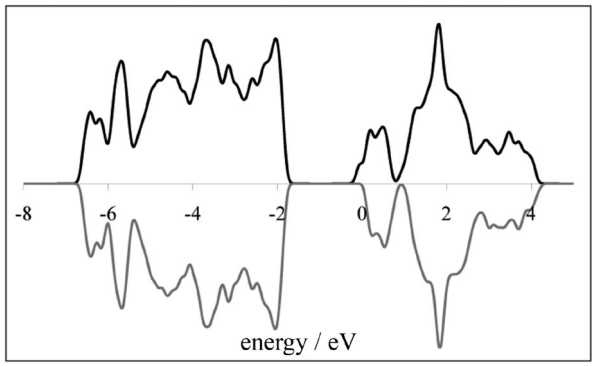

Figure 3. GGA calculated electronic density of states for reduced V_2O_5 with an oxygen vacancy at the O1 site. The scale is zeroed at the uppermost occupied state.

and standard DFT methods do not account properly for these weak interactions,[52,53] a phenomenon noted in other DFT studies on layered structures.[54–56] The equilibrium V−O bond distances for the stoichiometric bulk using GGA and GGA+U are shown in Table 2 and illustrated in Figure 1. These results are consistent with both experimental values and previous DFT studies.[5,31,32]

Figure 2 shows the calculated electronic density of states (EDOS) for (a) the GGA calculation and (b) the GGA+U calculation of the stoichiometric V_2O_5 structure. The calculated band gap from the GGA calculation at 1.87 eV is below the experimentally determined value of ∼2.35 eV. The calculated band gap for the GGA+U calculation of 2.26 eV is a distinct improvement on the uncorrected GGA value, but is still a slight underestimation of the experimental value.

3.2. Reduced V_2O_5. All reduced V_2O_5 calculations were carried out on a 1 × 3 × 3 supercell of $V_{36}O_{89}$, with the defective systems therefore having the formal stoichiometry of $\sim V_2O_{4.95}$. The GGA EDOS for all the vacancies is very similar, and that for the O1 system is shown in Figure 3. For all three vacancies no gap state is observed between the valence and conduction bands, in disagreement with experimental data which show that a peak should appear at ∼1 eV above the valence band.[15,17] In all three cases the excess charge produced by reducing the system occupies the V 3d states lying at the bottom of the conduction band, which then crosses the Fermi level, giving a metallic system.

Figure 4 shows the spin densities associated with the excess charge for each of the three GGA optimized vacancies. In all three cases the excess charge is delocalized. In the O1 vacancy system the vanadium directly underneath the vacancy is displaced downward to form a V−O−V bond with the layer underneath (Figure 4a). The majority of the excess charge is found on these two vanadium atoms and the two vanadium atoms closest to these on both layers. Some residual delocalized charge is also evident on some of the neighboring vanadium atoms on both layers. This is consistent with previous GGA calculations.[32] For the O2 and O3 vacancies the excess charge is delocalized over the entire layer that contains the defect. Interestingly, in the cases of the O2 and O3 vacancies, only a small amount of charge resides on the vanadium atoms neighboring the vacancy where the excess electrons might have been expected to localize (Figure 4b−c). Instead the majority of the charge is spread around the other vanadium atoms in the defective layer.

The absence of a gap state in the EDOS for the three GGA calculations, and the delocalization of the charge density associated with occupied states at the bottom of the conduction band, are consistent with previous uncorrected DFT studies.[30,32] The results are, however, at variance with experimental data, which suggest a definite localization of the excess charge and the appearance of a corresponding state in the band gap.[15,17]

To correct for the qualitative disagreement between the GGA calculation and experiment these calculations were repeated by

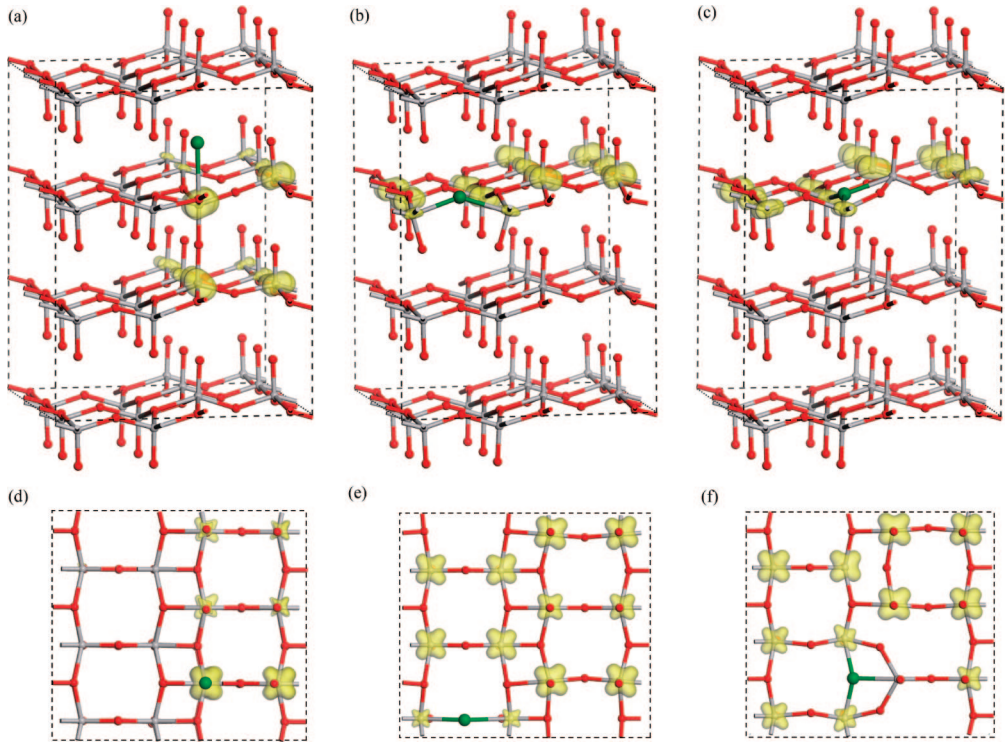

Figure 4. GGA calculated spin densities for reduced V_2O_5 with an oxygen vacancy at (a) the O1 site, (b) the O2 site, and (c) the O3 site. In each case both orthorhombic and plan views are shown (upper and lower panels), and the vacancy site is marked in green. The isosurface shown is set at 0.05 electrons $Å^{-3}$.

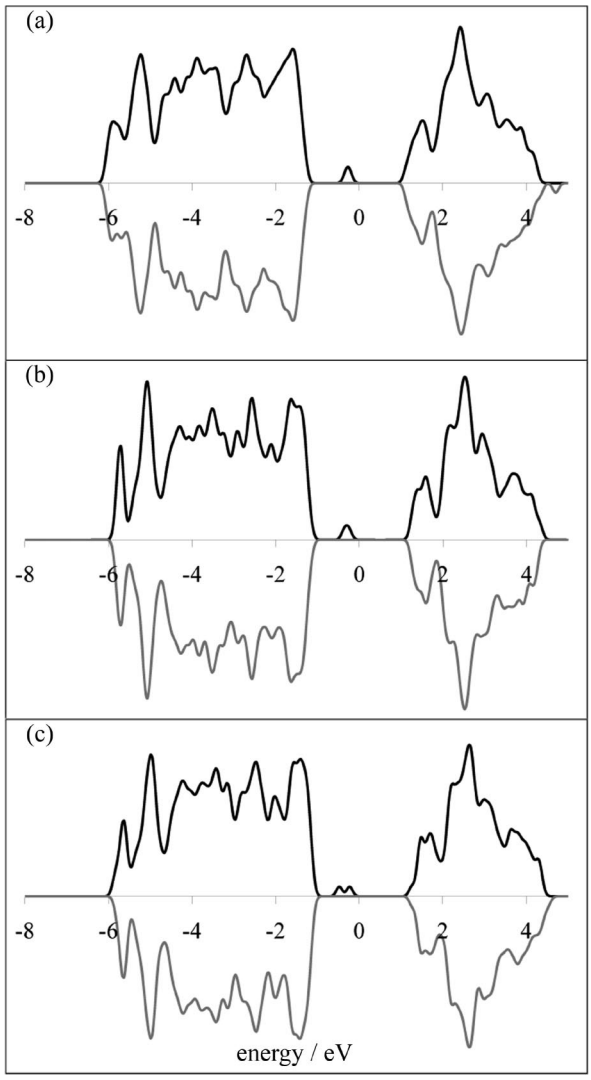

Figure 5. GGA+U (U = 4.0 eV) calculated densities of states for reduced V_2O_5 with oxygen vacancies at (a) the O1 site, (b) the O2 site, and (c) the O3 site. The zero of the energy scale is aligned with the highest occupied state; in each case this is the top of the gap state.

using the GGA+U approach. The underestimation of the band gap of pure V_2O_5 can be corrected to varying degrees by introducing the +U term. However, values of U large enough to recover the experimentally observed band gap do not give a distinct gap state, instead pulling the excess electron states into the valence band.[34] This is not surprising as this approach attempts to correct all of the shortcomings of DFT by correcting a single error, in this case the self-interaction of the d states of vanadium. Our chosen approach for selecting U is instead to use a value that gives the same ratio of the valence-band to gap-state:gap-state to conduction-band energies as is measured experimentally. This approach has been previously used to describe defect states in other oxides,[42,57] and here gives a value of U of 4.0 eV.

The EDOS for the GGA+U optimized structures for the O1, O2, and O3 vacancies are shown in Figure 5a−c. All three show a gap state between the valence and conduction bands. For the O1 vacancy (Figure 5a) the state lies ∼0.95 eV above the valence band. This is proportionately in the correct position between the valence-band maximum and the conduction-band minimum. The EDOS for O2 and O3 show gap states at ∼0.75 and ∼0.69 eV, respectively. The double peak in the EDOS for the O3 vacancy (Figure 5c) is attributed to a splitting caused by the in-phase and out-of-phase interaction due to the close proximity of the localized orbitals.

Figure 6a−c displays the geometry and spin density of the excess charge for the three vacancies. In agreement with previous DFT studies,[29–32] and the uncorrected GGA calculation described above, the creation of a vanadyl oxygen vacancy results in the formation of a V−O−V bond between the layers (Figure 5a). However, in contrast with uncorrected DFT results the spin density shows two localized electrons on the two neighboring V sites, formally giving V(IV), which is in agreement with previous interpretations of the UPS spectrum.[17] O2 and O3 vacancies yield localized electrons on the two vanadium sites neighboring the vacancy. The structural perturbation caused by the O2 and O3 vacancies in the GGA+U calculations is less than that obtained with GGA. For the O2 vacancy the neighboring vanadium atoms are 0.03 Å closer together and are displaced downward toward the layer below. For the O3 GGA+U vacancy the two neighboring vanadium atoms are moved toward one another by 0.14 Å relative to the O3 GGA vacancy calculation. These additional perturbations are primarily a consequence of the localization obtained with GGA+U, as the lower charge on the reduced V atoms leads to smaller V−V repulsion. The charge density associated with each atom can be estimated by projecting the charge onto atom-centered spherical harmonics, with radii of 1.2 and 1.55 Å for V and O, respectively. This gives approximate electron occupancies although it is subject to errors due to spatial overlap of the projection basis functions. For the bulk, this gives rise to valence occupations of 3.28 e for V (2.70 d electrons), 6.61 e for O1, 6.96 e for O2, and 7.21 e for O3. An additional 0.44 e is found for the reduced vanadium atoms in the O1 vacancy system, 0.43 e for the two vanadium atoms neighboring the O2 vacancy, and 0.50 e for the vanadium atoms neighboring the O3 vacancy. For each vacancy, the oxygens coordinated to the reduced vanadium atoms have ∼0.13 e located on them, and the integrated defect state charge densities of all other atoms in the three systems are below 0.05 e.

The energy of vacancy formation was calculated according to the equation

$$2V_V^x + O_O^x \rightarrow 2V_V^{'} + V_O^{\bullet\bullet} + \frac{1}{2}O_2$$

using Kroger−Vink notation; where $V_O^{\bullet\bullet}$ denotes the oxygen vacancy. The computed formation energies are listed in Table 3. O1 is the easiest vacancy to form in both the GGA and GGA+U calculations, in qualitative agreement with previous DFT studies,[31,32] and is in agreement with experimental findings.[10] The energies are not quantitatively the same, however, with the GGA+U results being 0.31, 0.46, and 0.30 eV more stable than the GGA calculated energies for the O1, O2, and O3 vacancies, respectively. It must be noted that our energetics are affected by the well-known inability of DFT to correctly describe the O_2 binding energy.[57–60] This error normally overstabilizes O_2 by as much as 0.7 eV with reference to experiment.[61] We have not applied any correction in this case, but this would have the effect of destabilizing each of the defect formation energies, by an amount independent of the specific oxygen vacancy type.

3.3. Intercalation. A second process entailing the reduction of V_2O_5 is Li intercalation. This is of particular interest as the intercalation of layered oxides has possible applications for energy storage applications. In addition to differences in the Madelung field between these two reduced classes of material,

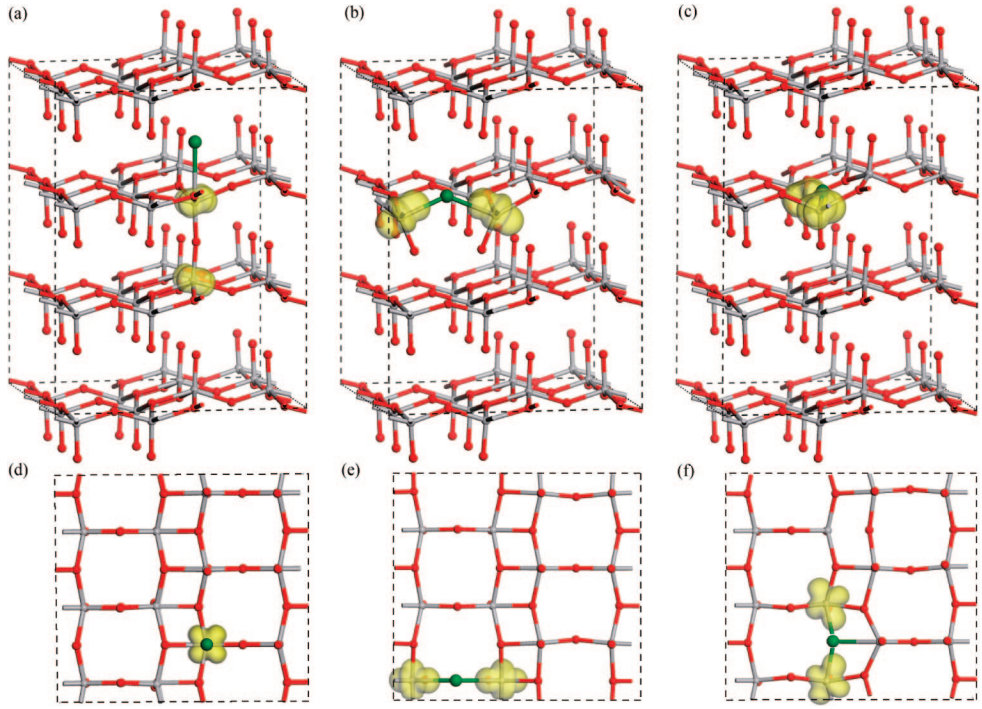

Figure 6. GGA+U (U = 4.0 eV) calculated spin densities for reduced V_2O_5 with an oxygen vacancy at (a) the O1 site, (b) the O2 site, and (c) the O3 site. In each case both orthorhombic and plan views are shown (upper and lower panels), and the vacancy site is marked in green. The isosurface shown is set at 0.05 electrons Å^{-3}.

TABLE 3: Energies of Formation of Oxygen Vacancies in Bulk V_2O_5[a]

energy of formation (eV)	GGA	GGA+U
O1vacancy	1.46	1.15
O2vacancy	3.15	2.69
O3vacancy	3.25	2.95

[a] All energies are given in eV.

TABLE 4: Calculated V−O Bond Distances for the Bulk γ-V_2O_5 Structure[a]

	Expt[28]	GGA[67]	GGA + U (this work)
$d_{V^a-O1^a}$	1.547	1.598 (+3.2%)	1.603(+3.6%)
$d_{V^a-O2^a}$	1.726	1.800 (+4.2%)	1.813(+5.0%)
$d_{V^a-O3^a}$	1.891	1.896 (+0.3%)	1.914(+1.2%)
$d_{V^a-O3'^a}$	1.986	2.034 (+2.4%)	2.020(+1.7%)
$d_{V^b-O1^b}$	1.581	1.598 (+1.1%)	1.602(+1.3%)
$d_{V^b-O2^b}$	1.847	1.799 (−2.6%)	1.808(−2.1%)
$d_{V^b-O3^b}$	1.896	1.902 (+0.6%)	1.921(+1.3%)
$d_{V^b-O3'^b}$	1.972	2.010 (+1.9%)	2.001(+1.4%)
$d_{V^a-O1^b}$	2.714	3.401 (+25.31)	3.097(+14.1%)

[a] All values are given in Å. The percentage values are given relative to the experimental value.

there are consequences for the electronic structure: O vacancies introduce an excess of two electrons per oxygen removed, whereas Li intercalation provides one additional electron per ion.

The local coordination environment of the vanadium atoms in the lithiated phases of V_2O_5 is similar to that in stoichiometric α-V_2O_5, with the structural differences arising from the relative orientation of VO_4 tetrahedra. For structures with large geometric differences significant variation of a suitable value of U might be expected. However, this is not the case for the reduced V_2O_5 systems considered here, and the localized V 3d states are likely to be equally well-described by a single value of U. Cococcioni and Gironcoli have used constrained−density-functional calculations and a linear response approach to predict ab initio values of U for the Fe 3d states in fayalite (Fe_2SiO_4),[62] where the Fe atoms occupy two inequivalent distorted octahedral sites, and obtained similar values (4.6 and 4.9 eV). We are able to examine the validity of the assumption of transferability of U among structurally related vanadium oxides by performing calculations of lithiated V_2O_5 phases using the value of U obtained from the oxygen-deficient systems described above, and comparing the resulting data with those obtained from XPS and UPS experiments.

The DFT+U (U = 4.0 eV) geometry and electronic structure of α-$Li_xV_2O_5$, with x = 0.028 (one Li per 18 formula units of V_2O_5), are shown in Figure 7. The Li intercalation causes only minimal perturbation of the stoichiometric V_2O_5 structure, with two vanadyl oxygens being pulled inward toward the lithium. The V−O bond lengths nearest the lithium change from 1.60 Å in the stoichiometric bulk to 1.66 and 1.64 Å in the α-$Li_xV_2O_5$ structure. The spin density plot (Figure 7b) shows that the extra electron provided by the Li is localized on the vanadium atom closest to the Li site. The EDOS shows the formation of a localized peak in the band gap at ~0.91 eV above the valence band (Figure 7c). This is consistent with recent UPS and XPS studies on Li intercalation into V_2O_5,[20] which show a V(IV) peak ~1 eV above the valence band.

The geometry and electronic structure of the γ phase of $Li_xV_2O_5$, for x = 1 (four Li in four formula units of V_2O_5), are shown in Figure 8. The perturbation caused by the Li intercalation is consistent with experimental observations.[21] Spin density plots (Figure 8a) show the localization of the four excess electrons on four of the eight vanadium sites, which is in agreement with previous crystallographic data reported by Galy et al. in which the presence of two distinct vanadium species was noted, formally attributed to V(V) and V(IV).[27] The calculated density of states (Figure 7b) shows a localized defect state in the band gap ~0.8 eV above the valence band, with a second peak ~0.44 eV above this. The double peak in the band

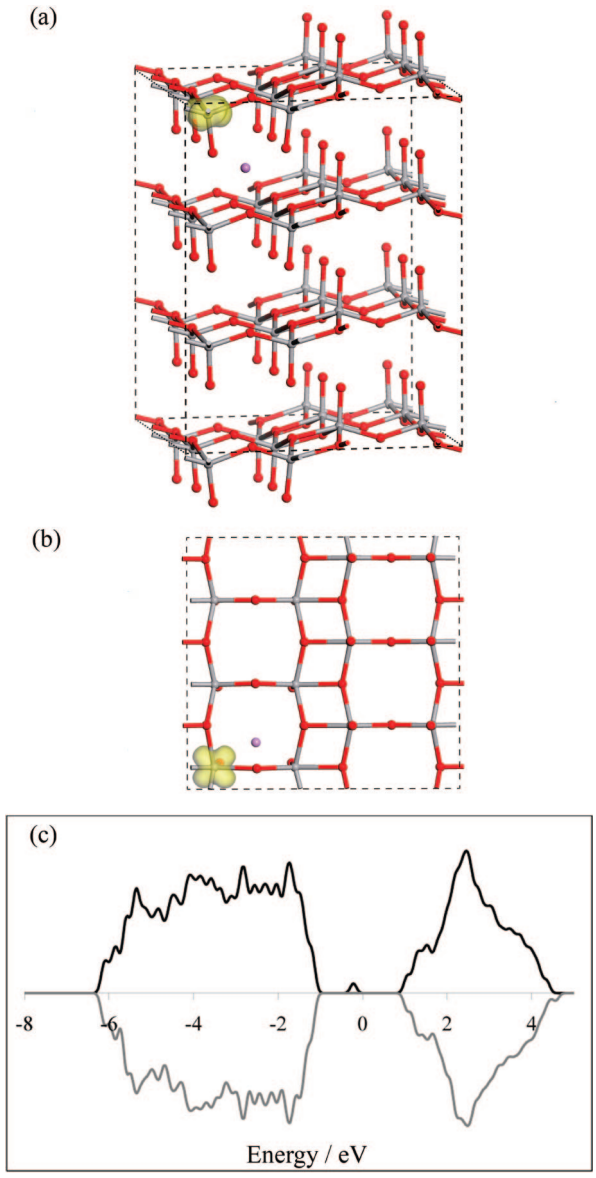

Figure 7. GGA+U (U = 4.0 eV) calculated geometry and electronic structure for α-$Li_xV_2O_5$ (x = 0.028). Parts a and b respectively show a side and plane view of the converged geometry, with the isosurface showing the spin density. The isosurface value is 0.05 electrons $Å^{-3}$. The Li atom is purple. Panel c shows the calculated DOS for this system. The zero of the energy scale is aligned with the uppermost occupied state.

gap in the EDOS is due to the close proximity of the localized orbitals along the c direction, giving rise to a disperse band that varies in energy along the Γ→Z vector of the Brillouin zone. This is consistent with the XPS and UPS study of Wu et al.,[20] which showed a V(IV) peak at ∼1 eV above the valence band.

The energetics of Li intercalation are calculated by using

$$V_V^x + Li_{(s)} \rightarrow V_V^{'} + Li_i^{\bullet}$$

again with Kroger−Vink notation. The energy of lithium intercalation from α-V_2O_5 to α-$Li_xV_2O_5$ was calculated to be −2.78 eV/Li, and that from α-V_2O_5 to γ-LiV_2O_5 was found to be −3.58 eV/Li. These energies are comparable to those obtained from previous theoretical intercalation studies on $LiMnO_2$ spinels, which report a value of −4.04 eV per Li dopant.[63]

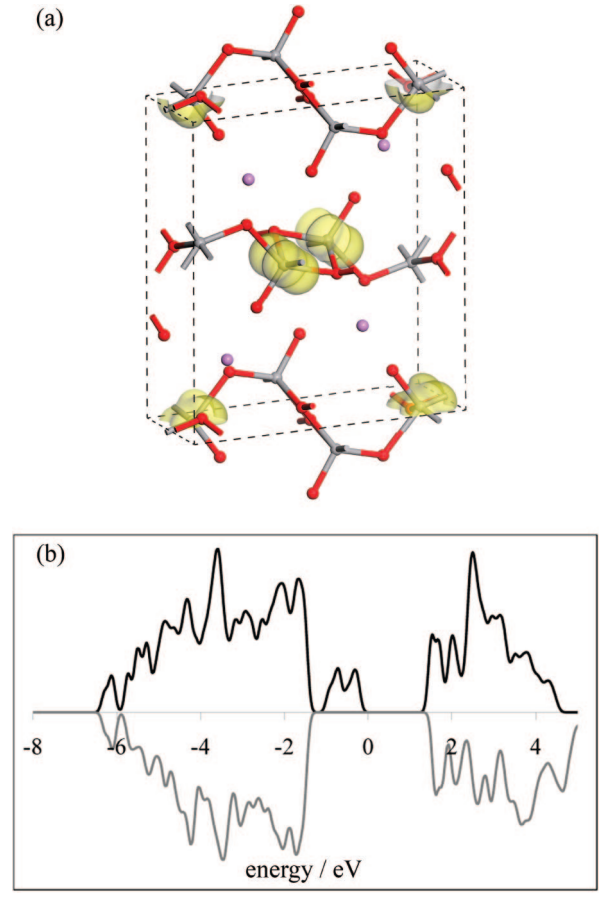

Figure 8. GGA+U (U = 4.0 eV) geometry and electronic structure for γ-LiV_2O_5. Panel a shows the converged geometry and the spin density. The lithium atoms are purple, and vanadium and oxygen atoms are red and gray, respectively. Panel b shows the DOS for the system, with the zero of the energy scale aligned with the top of the gap state

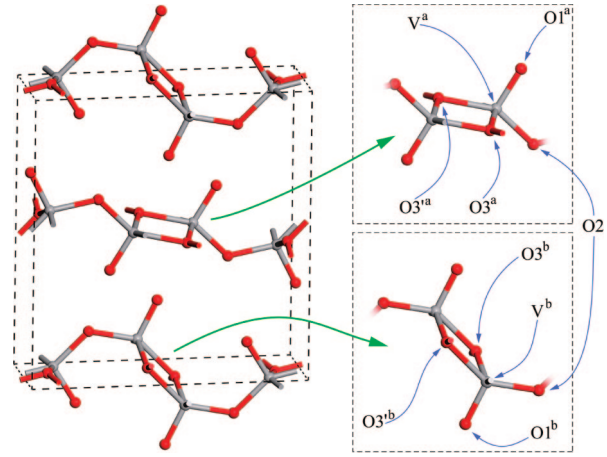

Figure 9. The GGA+U (U = 4.0 eV) calculated γ-V_2O_5 structure. γ-V_2O_5 can be constructed from two inequivalent V_2O_6 subunits, linked into chains by shared oxygen atoms (O2). The upper and lower right-hand panels show these two subunits, with the superscript used to denote which subunit atoms they are a part of. Note that O2 does not require a superscript since these atoms are shared between adjacent a and b subunits.

The α-V_2O_5 intercalation energy can be approximately equated to the V^{5+}/V^{4+} voltage, since the entropic and volume-change contributions to the change in free energy of the system are much smaller than the 0 K change in internal energy.[64] An improved estimate of the voltage would require a weighted

summation over multiple intercalation configurations at a given concentration, in the spirit of a stochastic Monte-Carlo process. Assuming that the Li−Li interaction is repulsive, and thus intercalated atoms will tend to maximize their distance from one another, the periodic arrangement in our calculation represents the lowest energy configuration for this concentration. Configurations with much smaller Li−Li distances will be higher in energy and are expected to contribute only a small amount to the voltage, while configurations with largely similar Li−Li distances but a small amount of thermal disorder when viewed in larger supercells are likely to be close in energy to the calculated system, since the concentration considered here is low; $x(\mathrm{Li}) = 0.028$. Less favorable intercalation configurations will, by definition, have higher energies and as such smaller lithium intercalation energies. Thus sampling these within a stochastic average will *reduce* the calculated voltage, making voltages based on a single lowest energy configuration an upper limit to a better sampled system. Our voltage of 2.78 V is in reasonable agreement with that observed in α-$Li_xV_2O_5$ by Moss et al.,[65] who reported a voltage of ~3.25 V with a metallic Li anode, in the limit of low Li concentration. Cell voltages for α-V_2O_5 coupled to a graphite anode will be slightly lower than those for Li metal since the energy of intercalation of Li from the liquid phase into graphite is ~0.16 eV.[66]

It has been demonstrated experimentally that upon lithium deintercalation of lithiated γ-LiV_2O_5, the system does not return to the α-V_2O_5 phase, but instead forms a metastable γ-V_2O_5 phase,[28] in contrast with all the lithiated phases formed for $0 < x < 1$. To investigate this metastable γ-V_2O_5 phase, all the Li atoms were removed from the relaxed γ-LiV_2O_5 geometry and a further geometry optimization was performed, resulting in the structure shown in Figure 9. The bond length and bond angles (see Table 4) are in good agreement with previous crystallographic[28] and DFT data.[67] The energy to intercalate this metastable phase was found to be −3.61 eV/Li. The larger energy of intercalation from γ-V_2O_5 to γ-LiV_2O_5 than from α-V_2O_5 to γ-LiV_2O_5 is to be expected, as the metastable γ-V_2O_5 phase is less stable than the pristine α-V_2O_5, thus making intercalation more favorable. Again, this intercalation energy can be used to estimate a voltage of 3.61 V versus metallic lithium. At this lithium concentration Li−Li interactions are likely to be energetically significant and our model can no longer be thought of as approximating an isolated cluster of interstitial sites. Instead this voltage corresponds to the contribution that would be made to a true stochastically determined voltage by a periodic array of Li interstitials, neglecting alternative disordered configurations, although these are likely to be higher in energy and therefore make a smaller contribution.

4. Conclusions

GGA-DFT and GGA+U have been employed to study the formation of the O1, O2, and O3 oxygen vacancies in bulk α-V_2O_5. The structural, electronic, and energetic features of each of these three vacancies have been described. In all cases, GGA predicts a metallic system, with the excess charge produced on creation of the oxygen vacancy delocalized over a number of vanadium centers close to the vacancy site. This metallic character is contrary to experimental findings, and consequently structural and energetic data are expected to be unrepresentative of the real system. Using GGA+U gives an improved description of these oxygen vacancies, which is in qualitative agreement with experimental USP and resPES studies. Vacancy formation is now found to lead to a localized reduction of the vanadium atoms neighboring the vacancies, which gives rise to a gap state in the calculated density of states.

The energetics of vacancy formation were also calculated, to determine which oxygen is the most likely to play a part in reduction of V_2O_5. Despite the failure of GGA to accurately describe the electronic structure of the oxygen-deficient system, GGA and GGA+U results show the same qualitative trend in the vacancy formation energies, with the O1 vacancy being the most stable defect, and thus the most likely to be active during reduction. However, the GGA+U energetics are quantitatively at variance with the GGA results, being considerably under stabilized.

The structure and energetics of Li intercalation in bulk V_2O_5 were considered at the GGA+U level, with the U value of 4.0 eV obtained from the calculations of the oxygen-deficient α-V_2O_5 system. Both the α- and γ- phases of $Li_xV_2O_5$ were examined. Again, localized gap states were observed in the calculated DOS, with positions in good agreement with experimental data, demonstrating a good degree of transferability of this value of U among structurally related V_2O_5 phases. The calculated energies of Li insertion were found to be −2.78 eV/Li from V_2O_5 to α-$Li_xV_2O_5$, and −3.58 eV/Li from V_2O_5 to γ-LiV_2O_5. To study the metastable γ-V_2O_5 phase, the inserted lithium atoms were then removed from the γ-LiV_2O_5 system and the structure was allowed to relax. The resulting equilibrium structure was in good agreement with the experimentally determined γ-V_2O_5 phase. Li intercalation energies were used to approximate open cell voltages at the Li concentrations considered in α- and γ-V_2O_5, giving values of 2.78 ($x = 0.028$) and 3.61 V ($x = 1$), respectively.

Acknowledgment. Support for this work was provided by Science Foundation Ireland (Grant nos. 04/BR/C0216 and 05/RFP/CHE0035) and the HEA for the IITAC PRTLI (Cycle III) grant. Computer resources were provided by the MOTT2 facility (EPSRC Grant GR/S84415/01) run by the STFC e-Science Centre and the IITAC supercomputer, as maintained by TCHPC.

References and Notes

(1) Mars, P.; Maessen, J. G. H. *J. Catal.* **1968**, *10*, 1–103.
(2) Whittingham, M. S. *J. Electrochem. Soc.* **1977**, *124*, C141−C141.
(3) Chain, E. E. *Appl. Opt.* **1991**, *30*, 2782.
(4) Van Hieu, N.; Lichtman, D. *J. Vac. Sci. Technol.* **1981**, *18*, 49.
(5) Enjalbert, R.; Galy, J. *Acta Crystallogr. C* **1986**, *42*, 1813–1815.
(6) Germain, J. E. In *Adsorption and Catalysis on Oxide Surfaces*; Che, M., Bond, G. C., Eds.; Elsevier: Amsterdam, The Netherlands, 1985; p 355.
(7) Creaser, D.; Andersson, B.; Hudgins, R. R.; Silveston, P. L. *Appl. Catal., A* **1999**, *187*, 147–160.
(8) Mamedov, E. A.; Cortes Corberan, V. *Appl. Catal., A* **1995**, *127*, 1–40.
(9) Kofstad, P. In *Nonstoichiometry, Diffusion and Electrical Conductivity in Binary Metal Oxides*; R. F. Krieger: Malabar, FL, 1983; p 57.
(10) Tamare, K.; Yoshida, S.; Ishida, S.; Kakioka, H. *Bull. Chem. Soc. Jpn.* **1968**, *41*, 2840–2845.
(11) Eon, J. G.; Olier, R.; Volta, J. C. *J. Catal.* **1994**, *145*, 318–326.
(12) Ramirez, R.; Casal, B.; Utrera, L.; Ruiz-Hitzky, E. *J. Phys. Chem.* **1990**, *94*, 8960–8965.
(13) Devriendt, K.; Poelman, H.; Fiermans, L.; Creten, G.; Froment, G. F. *Surf. Sci.* **1996**, *352−354*, 750–754.
(14) Goschke, R. A.; Vey, K.; Maier, M.; Walter, U.; Goering, E.; Klemm, M.; Horn, S. *Surf. Sci.* **1996**, *348*, 305–310.
(15) Hermann, K.; Witko, M.; Druzinic, R.; Chakrabarti, A.; Tepper, B.; Elsner, M.; Gorschluter, A.; Kuhlenbeck, H.; Freund, H. J. *J. Electron Spectrosc. Relat. Phenom.* **1999**, *98−99*, 245–256.
(16) Su, D. S.; Wieske, M.; Beckmann, E.; Blume, A.; Mestl, G.; Schlogl, R. *Catal. Lett.* **2001**, *75*, 81.
(17) Wu, Q. H.; Thissen, A.; Jaegermann, W.; Liu, M. L. *Appl. Surf. Sci.* **2004**, *236*, 473–478.
(18) Murphy, D. W.; Christian, P. A.; DiSalvo, F. J.; Waszczak, J. V. *Inorg. Chem.* **1979**, *18*, 2800–2803.
(19) Whittingham, M. S. *J. Electrochem. Soc.* **1976**, *123*, 315–320.
(20) Wu, Q. H.; Thissen, A.; Jaegermann, W. *Surf. Sci.* **2005**, *578*, 203–212.

(21) Cocciantelli, J. M.; Doumerc, J. P.; Pouchard, M.; Broussely, M.; Labat, J. *J. Power Sources* **1991**, *34*, 103–111.
(22) Dickens, P. G.; French, S. J.; Hight, A. T.; Pye, M. F. *Mater. Res. Bull.* **1979**, *14*, 1295–1299.
(23) Galy, J. *J. Solid State Chem.* **1992**, *100*, 229–245.
(24) Galy, J.; Darriet, J.; Hagenmuller, P. *Rev. Chim. Miner.* **1971**, *8*, 509.
(25) Rozier, P.; Savariault, J.-M.; Galy, J.; Marichal, C.; Horschinger, J.; Granger, P. *Eur. J. Solid State Inorg. Chem.* **1996**, *33*, 1.
(26) Rao, K. J.; Pecquenard, P.; Gies, A.; Levasseur, A.; Etourneau, J. *Bull. Mater. Sci.* **2006**, *29*, 535–546.
(27) Satto, C.; Sciau, P.; Dooryhee, E.; Galy, J.; Millet, P. *J. Solid State Chem.* **1999**, *146*, 103–109.
(28) Cocciantelli, J. M.; Gravereau, P.; Doumerc, J. P.; Pouchard, M.; Hagenmuller, P. *J. Solid State Chem.* **1991**, *93*, 497–502.
(29) Hermann, K.; Witko, M.; Druzinic, R. *Faraday Discuss.* **1999**, *114*, 53–56.
(30) Hermann, K.; Witko, M.; Druzinic, R.; Tokarz, R. *Appl. Phys. A: Mater. Sci. Process.* **2001**, *72*, 429–442.
(31) Sauer, J.; Dobler, J. *Dalton Trans.* **2004**, 3116–3121.
(32) Ganduglia-Pirovano, M. V.; Sauer, J. *Phys. Rev. B* **2004**, *70*, 045422-13.
(33) Lambrecht, W.; Djafari-Rouhani, B.; Vennik, J. *Solid State Commun.* **1981**, *39*, 257–261.
(34) Laubach, S.; Schmidt, P. C.; Thissen, A.; Fernandez-Madrigal, F. J.; Wu, Q. H.; Jaegermann, W.; Klemm, M.; Horn, S. *Phys. Chem. Chem. Phys.* **2007**, *9*, 2564–2576.
(35) Ganduglia-Pirovano, M. V.; Hofmann, A.; Sauer, J. *Surf. Sci. Rep.* **2007**, *62*, 219–270.
(36) Jiang, J.; Wang, Z.; Chen, L. *J. Phys. Chem. C* **2007**, *111*, 10707–10711.
(37) Nolan, M.; Watson, G. W. *Surf. Sci.* **2005**, *586*, 25–37.
(38) Scanlon, D. O.; Walsh, A.; Morgan, B. J.; Nolan, M.; Fearon, J.; Watson, G. W. *J. Phys. Chem. C* **2007**, *111*, 7971–7979.
(39) Sieberer, M.; Redinger, J.; Mohn, P. *Phys. Rev. B* **2007**, *75*, 035203.
(40) Nolan, M.; Grigoleit, S.; Sayle, D. C.; Parker, S. C.; Watson, G. W. *Surf. Sci.* **2005**, *576*, 217–229.
(41) Coquet, R.; Willock, D. J. *Phys. Chem. Chem. Phys.* **2005**, *7*, 3819–3828.
(42) Morgan, B. J.; Watson, G. W. *Surf. Sci.* **2007**, *601*, 5034–5041.
(43) Ackermann, L.; Gale, J. D.; Catlow, C. R. A. *J. Phys. Chem. B* **1997**, *101*, 10028–10034.
(44) Anisimov, V. I.; Zaanen, J.; Andersen, O. K. *Phys. Rev. B* **1991**, *44*, 943.
(45) Dudarev, S. L.; Botton, G. A.; Savrasov, S. Y.; Humphreys, C. J.; Sutton, A. P. *Phys. Rev. B* **1998**, *57*, 1505.
(46) Shick, A. B.; Pickett, W. E.; Liechtenstein, A. I. *J. Electron Spectrosc. Relat. Phenom.* **2001**, *114*−*116*, 753–758.
(47) Kresse, G.; Furthmuller, J. *Comput. Mater. Sci.* **1996**, *6*, 15–50.
(48) Kresse, G.; Hafner, J. *Phys. Rev. B* **1994**, *49*, 14251.
(49) Perdew, J. P.; Burke, K.; Ernzerhof, M. *Phys. Rev. Lett.* **1996**, *77*, 3865.
(50) Blöchl, P. E. *Phys. Rev. B* **1994**, *50*, 17953.
(51) Murnaghan, F. D. *PNAS* **1944**, *30*, 244–247.
(52) Rydberg, H.; Dion, M.; Jacobson, N.; Schröder, E.; Hyldgaard, P.; Simak, S. I.; Langreth, D. C.; Lundqvist, B. I. *Phys. Rev. Lett.* **2003**, *91*, 126402.
(53) Tsuzuki, S.; Luthi, H. P. *J. Chem. Phys.* **2001**, *114*, 3949–3957.
(54) Walsh, A.; Watson, G. W. *Phys. Rev. B* **2004**, *70*, 235114-7.
(55) Walsh, A.; Watson, G. W. *J. Phys. Chem. B* **2005**, *109*, 18868–18875.
(56) Walsh, A.; Watson, G. W. *J. Solid State Chem.* **2005**, *178*, 1422–1428.
(57) Nolan, M.; Parker, S. C.; Watson, G. W. *Surf. Sci.* **2005**, *595*, 223–232.
(58) Curtiss, L. A.; Raghavachari, K.; Redfern, P. C.; Pople, J. A. *J. Chem. Phys.* **1997**, *106*, 1063–1079.
(59) Hammer, B.; Hansen, L. B.; Nørskov, J. K. *Phys. Rev. B* **1999**, *59*, 7413.
(60) Johnson, B. G.; Gill, P. M. W.; Pople, J. A. *J. Chem. Phys.* **1993**, *98*, 5612–5626.
(61) *CRC Handbook of Chemistry and Physics*, 67th ed.;Weast, R. C., Ed.; CRC Press: Boca Raton, FL, 1987.
(62) Cococcioni, M.; de Gironcoli, S. *Phys. Rev. B* **2005**, *71*, 035105.
(63) Ning, L. C.; Wu, J. P.; Zhou, C. G.; Yao, S. J.; Pi, Z. B.; Cheng, H. S. *Int. J. Quantum Chem.* **2007**, *107*, 225–231.
(64) Aydinol, M. K.; Kohan, A. F.; Ceder, G.; Cho, K.; Joannopoulus, J. *Phys. Rev. B* **1997**, *56*, 1354–1365.
(65) Moss, P. L.; Fu, R.; Au, G.; Plichta, E. J.; Xin, Y.; Zheng, J. P. *J. Power Sources* **2003**, *124*, 261–265.
(66) Kganyago, K. R.; Ngoepe, P. E.; Catlow, C. R. A. *Solid State Ionics* **2003**, *159*, 21–23.
(67) Willinger, M.; Pinna, N.; Su, D. S.; Schlogl, R. *Phys. Rev. B* **2004**, *69*, 155114-7.

JP711334F